Vol. 19, No. 2 (2020) 677-689
Revista Mexicana de Ingeniería Química

Thermal study of a solar distiller using computational fluid dynamics (CFD)

Estudio térmico de un destilador solar usando dinámica de fluidos computacional (CFD)

R.J. García-Chávez[1], A.U. Chávez-Ramírez[1], H.I. Villafán-Vidales[2], J.B. Velázquez-Fernández[3], I.P. Hernández-Rosales[4]*

[1] *Centro de Investigación y Desarrollo Tecnológico en Electroquímica*
[2] *Instituto de Energías Renovables, UNAM*
[3] *Centro de Investigación y Asistencia en Tecnología y Diseño del Estado de Jalisco.*
[4] *Universidad Autónoma de Nayarit*

Received: July 1, 2019; Accepted: October 2, 2019

Abstract

This study presents the design, modeling and behavior of a solar distiller using Computational Fluid Dynamics (CFD). The measured parameters are: 1) behavior of the internal temperature, 2) cover and volume generated after the solar distillation process, 3) the transfer coefficients obtained during the months of operation. The main results indicate that the month of May has the highest average water temperature in the interior with 44 ºC and the highest production of distilled water with an average of 1000 ml per day. The same month had an average of incident global radiation per day of 5.8 kWh / m^2 which is the highest among the months of operation. The model of Kumar and Tiwari is applied to study the thermal behavior of the solar distiller. In order to determine the drinkability of distilled water, the water quality analyses were carried out, and it was found that the water meets the NOM-127-SSA1-1994 standard. Thus, the clean water was obtained at the same time from the designed system under real weather conditions.

Keywords: solar thermal energy, convection, heat transference, energetic balance.

Resumen

Este estudio presenta el diseño, el modelado y el comportamiento de un destilador solar utilizando Computational Fluid Dynamics (CFD). Los parámetros medidos son: 1) el comportamiento de la temperatura interna, 2) la cantidad de cobertura y volumen generada después del proceso de destilación solar, 3) los coeficientes de transferencia obtenidos durante los meses de operación. Los principales resultados indican que el mes de mayo tiene la temperatura promedio más alta del agua en el interior con 44 ºC y la mayor producción de agua destilada con un promedio de 1000 ml por día. El mismo mes tuvo un promedio de radiación global incidente por día de 5.8 kWh /m^2, que es el más alto entre los meses de operación. Se aplica el modelo de Kumar y Tiwari para estudiar el comportamiento térmico del destilador solar. Para determinar la capacidad de beber del agua destilada, se realizaron los análisis de laboratorio y se encontró que el agua cumple con la norma NOM-127-SSA1-1994. Por lo tanto, el agua limpia se obtuvo al mismo tiempo del sistema diseñado en condiciones climáticas reales.

Palabras clave: energía solar térmica, coeficiente de calor, balance de energía.

1 Introduction

Mexico has renewable water reserves. However, the distribution of these reserves is not uniform throughout the country, for example, while the southern states have 26.1% of the population, they also have the greater rainwater availability percentage of 68.26%. These data reflect the great hydrological stress for the northern regions within which the greatest industrial activity of Mexico is located (CONAGUA, 2012). Other coastal regions have large water volumes but with high concentrations of salt, thus they cannot be considered as sources of drinking water (PNUMA, 2012). With the increase of the population and over exploitation and excessive extraction of water resources, the reserves of this vital liquid are affected and particularly the arid and semi-arid zones. This brings negative impacts on the biotic resources. The reserves are decreasing at a rate of 6 km^3/ year, where the main causes are the usage in the agricultural sectors with more than 70%, the usage in the industry sectors with 5% and the usage in the

* *Corresponding author. E-mail*: paz.rosales@gmail.com
https://doi.org/10.24275/rmiq/IE671
issn-e: 2395-8472

public sector which consumes 14% (Reyes-Vidal *et al*., 2012).

In order to obtain new fresh water sources, seawater desalinization technologies have been developed in potable regions with low water availability using different processes and energy sources. Solar distillation (SD) is a technique that uses renewable energy from the sun, which defines it as a low environmental impact technology. Passive solar distillation can provide potable water for agricultural and domestic activities in regions with solar resources with an average production with an average production of 2-3 L/day (Sampathkumar *et al*., 2010).

However, SD is facing great problems in being applied at the large scale, therefore, one of the main objectives of this research in the area was to increase the efficiency and production of distillation, which depends on the prototype design factors, such as properties of construction materials, inclination angle and cover transmittance, equipment volume, temperature and feeding water salinity (Ranjan & Kaushik, 2013). It also depends on the meteorological parameters, such as global radiation, air temperature, wind direction and moisture (Ranjan & Kaushik, 2013).

Modeling is an important tool that allows the improvement of prototypes in order to enhance the productivity of distilled water. For example, Khare, V. R *et al*. 2017 propose a model of passive solar distiller along with the "FLUENT-ANSYS" package. They evaluate a day of operation where the mass fraction of distilled volume is determined and it is 2.0 at 14 h and 0.9 in 8 h of operation. The steam temperature generated by the equipment is determined afterwards. The maximum temperature obtained in simulation is 87 °C and in experimentation is 72 °C (Khare *et al*., 2017). Rajesh Tripathi y Tiwari in 2006 performed computational modeling using the Matlab tool in order to predict the convective coefficients. There was a production of water of 0.856 kg/m^2 per day (Tripathi & Tiwari, 2006) Al Narjes Setoodeh (2011) reported a CFD simulation for a passive solar distiller in the Springtime using the constants reported by Kumar and Tiwari in 1996 where the convective transfer coefficients were evaluated (V. Dunkle, 1961; Kumar & Tiwari, 1996). Nader Rahbar *et al*. (2015) performed a CFD simulation in a 2D geometry, where heat and mass transfer were evaluated in a solar distillation tube. The simulation showed acceptable results that were comparable to those reported in the body of literature and the researchers proposed new relations for obtaining the transfer coefficients of heat and mass (Tsilingiris, 2013).

Different authors have studied how to increase the performance of solar desalination systems, through forced water circulation and the addition of nano particles to increase the thermal properties of the fluid. Water recirculation favors the increase in temperature and therefore increases evaporation. Currently, the coupling with external sources is studied to increase efficiency, such as heating systems through collectors, heat exchangers and the addition of nano particles (Singh *et al*., 2018). A thermal photovoltaic system can generate the energy required by the pump to force the water flow to recirculate.

Sing *et al*. (2018), carried out a review on the efficiency and performance of different designs of solar distillation (DS) technology. It provides information collected from the research of different authors studying energy matrices of the DS that provide a study on the energy recovery time, energy production factor, life cycle conversion efficiency, thus pointing out the limitations of DS technology (Singh *et al*., 2018).

Sing *et al*. (2019), presented a review on the efficiency of passive DS designs with modifications that improve performance based on efficiency, productivity and technology, as well as commercial, domestic and portable DS with designs other than conventional DS (Singh *et al*., 2019).

Elashmawy (2017) conducted a study with three combinations (I) TSS filled with wet black cloth with brackish water, (II) TSS without cloth and (III) with compound parabolic solar concentrator, with efficiencies of 36.5%, 30.5% y 28.5% (Elashmawy, 2017). Rahbar *et al*. (2018) experimented with tubular DS geometries, with a tubular cylindrical chamber and a partially triangular tubular chamber. An analysis and CFD simulation were performed and compared with experimental results yielding 35% and 41% (Rahbar *et al*., 2018). Rashidi *et al*. (2018) carried out an experimentation of a DS with type V fund with porous media. Efficiency, productivity and economy were determined with an increase in production of 17% compared to conventional DS (Rashidi *et al*., 2018).

Other authors conducted studies based on non-conventional designs with the objective of increasing the performance and the distillate production. Kaushal *et al*. (2017) carried out a study on a multiple effect diffusion solar still with waste heat recovery, where heat retained by brackish water is reused at the output to heat feed water in the following effect (Kaushal *et al*., 2017). Al Nimr and Daholan (2015) showed an advanced tubular system with a parabolic trough

concentrator and a storage tank. The tube has a porous internal surface; the collector offers more surface area to receive more solar radiation, increases the temperature and produces greater volume (Al-Nimr & Dahdolan, 2015). Hansen and Murugovel (2017) presented a combination of distillers with single slope in series in a staggered manner. This system collects the distillates of each stills, the system has a unique cover with a larger area of condensation (Samuel Hansen & Kalidasa Murugavel, 2017).

In the present work, a CFD simulation with Wall Condensation Model in is described, where the temperature behavior in the glass and the internal system of the equipment are calculated and also, a comparison is made between the simulation and experimental results regarding water temperature, glass temperature and convective heat transfer coefficient, obtained during the six months period of investigation.

2 Materials and methods

2.1 Materials

The passive solar distiller consists of a galvanized steel container with base area of 1 m^2 and height of 0.5 m in the back and 0.14 m in the front. The container is covered with fiberglass-based insulation with thickness of 2 mm in order to reduce heat losses. The internal walls of the container are painted with a black epoxy, in order to increase the absorptivity of the radiation, to reduce heat losses by radiation and to avoid corrosion by seawater. The top of the solar distiller is covered with a high-transmittance glass of 3 mm thickness as cover. The slope of the deck was 19.5 degrees, it was based on geographic latitude of the city of Tepic, where the cover may be ± 2 °, the equipment is oriented from north to south, with the aim of taking advantage of solar radiation more homogeneously throughout a day of operation. The prototype was installed at the Autonomous University of Nayarit, Mexico at a latitude of 21.5° and a longitude of -104.89° (Figure 1).

2.2 Simulation

The simulation of the solar distiller was based on the evaporation and condensation process. This was done with the software ANSYS 17.1, CFX package and

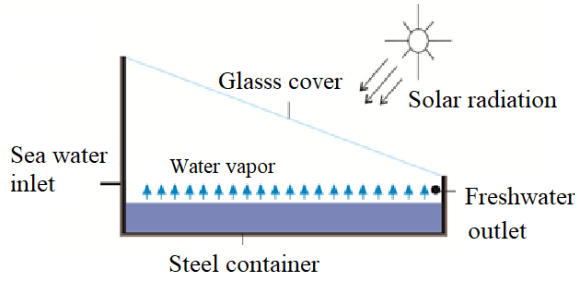

a)

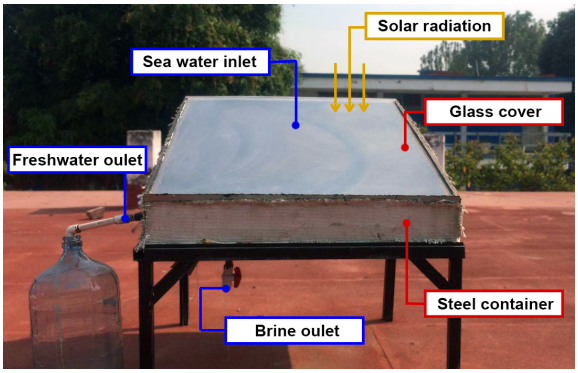

b)

Figure 1. a) Solar distillation. b) Solar distillation equipment.

the "wall condensation" model. Boundary conditions were applied in the domain of the fluid to solve the equations of continuity, momentum and energy (Guide, 2012; Tutorials, 2015).

CFX simulations were solved in 3 stages: problem definition, solution and analysis of results. In the problem definition, it is necessary to consider the transport equations, which govern the phenomenon as well as its initial and boundary conditions (Gomez-Daza & Ochoa-Martinez, 2011; Tutorials, 2015). Equation 1 shows the continuity equation, equation 2 represents the momentum and the energy equation is on equation 3.

$$\frac{\partial \rho}{\partial t} + \nabla \cdot (\rho \mathbf{U}) = 0 \tag{1}$$

$$\rho \frac{\partial \mathbf{U}}{\partial t} + \rho \mathbf{U} \cdot \nabla \mathbf{U} = \nabla \cdot \boldsymbol{\sigma} + \mathbf{B} \tag{2}$$

$$\rho \frac{\partial H}{\partial t} + \rho \mathbf{U} \cdot \nabla H = \nabla \cdot (\lambda \nabla T) + \frac{\partial p}{\partial t} \tag{3}$$

Where: ρ is the fluid density, U is the velocity vector, $\boldsymbol{\sigma}$ is the stress tensor, $\mathbf{B} = \mathbf{g}$ is the body strength (Pa/m), p is the pressure, $\mathbf{g}$ is the gravity vector.

The domain consists of two phases for liquid water and for a mixture of steam and air. A laminar boundary layer model was used in the glass section and the cover temperature was taken as the condensate temperature.

The laminar boundary layer consists of molar flows J_A and J_B, where A represents a non-condensable component and B a condensable component (Guide, 2012). The mathematical model of the CFD simulation resolution with the preloaded Wall-condensation CFX-ANSYS model is represented from equation 5 to 7 (Guide, 2012) and (Tutorials, 2015).

$$J_A = J_m X_A - D_{AB} C_m \frac{\partial X_A}{\partial y} = 0 \tag{4}$$

$$J_B = J_m X_B - D_{AB} C_m \frac{\partial X_B}{\partial y} \tag{5}$$

$$M_B = W_B J_B m_B \ln\left[\frac{1 - X_B(\delta)}{1 - X_B(0)}\right] \tag{6}$$

$$m_B = \frac{D_{AB}}{W_m} \frac{D_{AB}\rho_m}{\delta} \tag{7}$$

where: J_A is a molar flow of the A component, J_B is the molar flow of the B component, J_m is the molar convective flow of the mixture, C_m is the molar density of the mixture, X_A is the non-condensable molar fraction, X_B is the condensable molar fraction, D_{AB} is the binary diffusion coefficient, y is the distance from the condenser wall, δ is the width of the boundary layer and ρ_m is the mixture density.

The condensable fraction is determined from the assumption that the steam is in thermal equilibrium with the liquid-vapor interface. The vapor in the boundary layer will be wet, supersaturated or a type of fog, however, only dry steam drives the concentration gradient of the condensable flow. For this reason, the molar fraction of dry steam is used to determine the condensed mass fraction from the boundary layer, which is represented in equation 5 (Guide, 2012; Tutorials, 2015).

$$X_B(\delta) = \min[X_b(\delta), X_{B,sat}(\delta)] \tag{8}$$

Where: $X_{B,sat}$ is the saturated molar fraction.

2.2.1 Meshing details

The geometry of the 3D distillation equipment was modeled with the aforementioned CFX Wall Condensation Model. A mesh with a tetrahedral coupling was used with 11,986 nodes and 60,580 elements (Figure 2). Verification was made of a mesh independence with different sizes, a rough

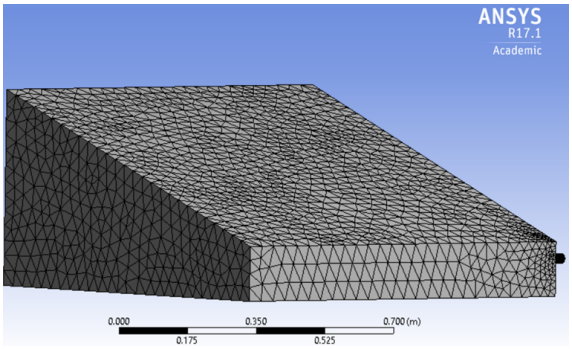

Figure 2. Mesh used in simulations.

tetrahedral mesh of 29,744 elements and a fine mesh of 138,608 elements. When performing the corresponding simulations, the results of the three meshes are similar with a difference of 0.03% in all three cases which is negligible and indicates that the mesh type does not affect the solution of the simulation.

Wall Condensation Model. The solar distiller inlets and outlets are modeled as fluid domains. In the developed.

The computational modeling of the solar distiller was carried out using the CFX model the following points are assumed: there were no convective losses of the System to the environment, and the water feed temperature was at room temperature of 24 ºC. It was also assumed that the temperature of the walls behaved homogeneously throughout the plate. The model was used to calculate the internal temperature that reaches the equipment and the average amount of distillate generated.

2.3 Correlation coefficients "R"

During the experiments, it was prepared a dispersion diagram per month on the three variables studied, in order to directly visualize the degree and type of association between these parameters, in particular the correlation coefficient R.

A statistical correlation allows knowing if a variable is accompanied by a change in another variable, then it is said that both variables are correlated, their value varies from -1 to 1, which indicates the strength of relationship that exists between the variables. In the present work the correlation coefficient was calculated for the internal temperature, crystal and the amount of volume, each of them with respect to the incident radiation, were calculated and are presented in Table 2.

Table 1. Wind speed in Tepic.

Month	Wind speed m/s
November	2.02
December	1.85
January	1.95
February	2.06
March	2.47
April	2.54
May	2.75

2.4 Energy balance

The solar distillation processes perform a series of physical phenomena that intervene in the functioning of the equipment. Therefore, there is a heat transfer coefficient in each one of them.

The energy balance in the equipment is provided in three parts: energy balance in the cover, in the container, and in water. The summative assessment of these three parts comprises the global energy balance in a distiller. (Susana Fonseca, Eider Miranda, & Torres, 2012) reports an equation for the energy balance in the different stages in the equipment. According to the abovementioned simplifications the energy balances are the following:

2.4.1 Energy balance in the glass cover

The glass cover has a high transmissivity index; this allows the incident radiation to enter in large part towards the solar distillation in the form of radiation. However, the emissivity of the material and the convection that occurs in the environment decrease the useful heat (Sampathkumar *et al*., 2010). The above is represented in the following equations:

$$m_g Cp_g \frac{dT}{dt} = \alpha_1 H_s + h_1(T_w - T_g) - h_2(T_g - T_e) \quad (9)$$

Where: m_g is the mass of glass, Cp_g is the specific heat of the glass, H_s is the incident radiation, α_1 is the absorption coefficient, h_1 is the transfer coefficient between glass and water, T_w is water temperature, T_g is glass temperature, h_2 the transfer coefficient between the glass and the environment and, T_e is the environmental temperature.

$$q_1 = 0.016273(P_w - P_g)h_1 \quad (10)$$

The convective coefficient (h_1) is calculated using the model proposed by Dunkle (1961), (Kumar & Tiwari, 1996; Tsilingiris, 2013; Al-Sulttani *et al*., 2017) which is valid for $Gr = 1.794\times10^6$ to 5.724×10^7 for $Ra = 10^7$ to 10^{11}:

$$h_1 = 0.0162(P_w - P_g)\frac{K_{air}}{L}0.0538(Gr * Pr)^{0.384} \quad (11)$$

Where L is the length of the container, K_{air} is the thermal conductivity of the humid air, Gr is the Grashof number and Pr represents the Prandlt number, $(Gr * Pr)$ is the Rayleigh number (Ra), and Nu is the Nusselt number for $Ra = 10^4$ to 10^9.

The saturation steam pressure at water temperature is obtained with the following correlation that explains the ratio of the temperature and pressure difference (Dunkle, CSIRO, Scientific, & Organization, 1961; Banat *et al*., 2002; Fernández & Chargoy, 1990; Rahbar *et al*., 2015):

$$P_w = \exp\left(25.317 - \frac{5144}{T_w + 273}\right) \quad (12)$$

The saturation steam pressure at steam temperature is calculated by using the following correlation (Banat *et al*., 2002; Dunkle *et al*., 1961; Fernández & Chargoy, 1990; Rahbar *et al*., 2015):

$$P_g = \exp\left(25.317 - \frac{5144}{T_g + 273}\right) \quad (13)$$

where: P_w is the saturated steam pressure at water temperature, P_g saturated steam pressure at glass temperature.

Table 2. Correlation coefficients "R" month by month with respect to incident radiation.

Month	Internal Temperature	Glass Temperature	Volume
November	0.83	0.77	0.82
December	0.89	0.71	0.85
January	0.81	0.88	0.8
February	0.89	0.8	0.84
March	0.8	0.89	0.87
April	0.96	0.87	0.8
May	0.84	0.75	0.88

The Grashof number is calculated using the following expression:

$$Gr = \frac{g\beta\rho^2 A\Delta T}{\mu^2} \quad (14)$$

where: β is the coefficient of volumetric expansion, ρ is the water density, A is the distiller area, ΔT is the temperature difference between water and glass, and μ is the dynamic viscosity.

β was calculated by assuming an ideal gas and this was corroborated with water properties tables obtained from (Çengel & Ghajar, 2011).

Investigations by Sharpley and Boetler showed that due to the differences in air molar masses, water steam and composition of the cover water mixture components and temperatures which the motor force that activates the circulation do not constitute the ordinary temperature difference $\Delta T = T_w - T_g$ that occurs in conventional thermal systems (Kumar & Tiwari, 1996; Sharpley *et al*., 1938). Malik *et al*. (1982) proposed ΔT used in the present work and which is presented in Eq. 15.

$$\Delta T = (T_w - T_g) + \left[\frac{(P_w - P_g)(T_w + 273)}{268.9 \times 10^3 - P_w}\right] \quad (15)$$

$$q_2 = h_2(T_g - T_e) \quad (16)$$

The convective coefficient between water and environment is represented by the following relation. This is valid when using $0 \leq v_z \leq 7$ m/s of wind speed and maximum Reynolds number of 10^6, (Duffie *et al*., 2013; Abdel-Rehim & Lasheen, 2005).

$$h_2 = 5.7 + 3v_z \quad (17)$$

The Reynolds number is calculated with the equation.

$$Re = \frac{v_z * l}{\nu} \quad (18)$$

where: v_z is the wind speed and ν is dynamic viscosity.

In table 1, the wind speed in Tepic Nayarit is shown, which was taken from the Internet portal of the National Institute of Forestry, Agriculture and Livestock Research (INIFAP, 2014; González, 2014).

2.4.2 *Energy balance in water*

The energy balance in water is obtained by the solar energy captured by the water, as from the energy transferred from the glass cover to the water and the energy transfer by convection of the container to the water, which is expressed in Eq. 19.

$$m_w Cp_w \frac{dT}{dt} = \alpha_2 H_s + h_3(T_c - T_w) - h_1(T_w - T_g) \quad (19)$$

where: H_s id the solar radiation, m_w is the water mass, Cp_w the specific heat of water, α_2 coefficient of absorption of the water, and T_g temperature of the glass cover crystal.

$$h_3 = Nu\left(\frac{K_a}{L_w}\right) \quad (20)$$

$$Nu = 0.037 * Re^{0.8} * (0.7282)^{1/3} \quad (21)$$

Where: K_a is the thermal conductivity of air and L_w is the inner length of the container, this Nusselt expression is used for number for Re with boundary conditions of 10^4 to 10^9 (Çengel & Ghajar, 2011).

The stages of the equipment where the heat transfer coefficients were evaluated were from the glass to the environment and the water and from the walls of the vessel to the water, which is at a height of 10 cm. The glass that works as a condenser receives incoming solar radiation which is the most important factor in passive solar distillation equipment, the glass transfers heat to the environment from the water and by its high transmissivity allows the heat to be absorbed by the walls of the equipment. Subsequently, the energy is transferred as heat to the water which raises its temperature until it reaches a vapor phase. In the case of glass, the convective coefficient was evaluated both towards the atmosphere (h_2) and towards the water (h_1), however, in CFX an assumption was made of a non-existent air current and was evaluated without heat transfer towards the outside. The steel vessel is isolated so that there is no heat transfer to the environment and it is taken as an adiabatic process, hence, only the heat transfer to the fluid with h_3 was evaluated. The water feed was performed at a rate of 0.005 m / s at an ambient temperature of 24 ºC and a mass fraction of 0.6, the remaining fraction was taken as air.

2.5 *Experimental method*

The solar distiller was operated at 8-hr daily intervals from 9:00 AM to 5:00 PM during the period from November 2016 to May 2017. The temperature on the cover glass was measured using “SPER SCIENTIFIC 800004 (0.5% uncertainty)" equipment and the temperature inside the distiller was monitored with a “CEM DT-811 (1% uncertainty)" infrared thermometer. Both temperatures were monitored every hour from 9:00 AM to 5:00 PM. The incident global radiation was measured with a pyrometer “Kipp & Zone, model CM11 (2% uncertainty)".

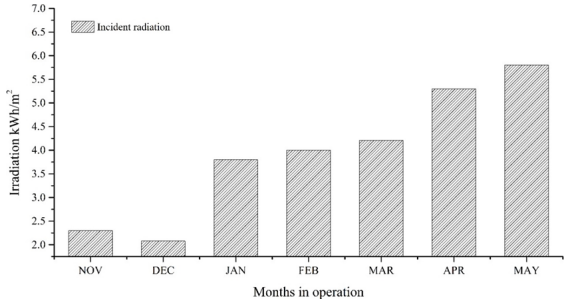

Figure 3. Incident radiation during the period of experimentation.

Finally, the still volume was measured daily in order to determine volume of water produced.

3 Results and discussion

In figure 3, global incident radiation during months of experimentation is shown. It can be observed that in May (5.84 kWh/m^2), maximum irradiances were achieved followed by April (5.3 kWh/m^2). The months that showed the lower amounts of global radiation were November and December with 2.3 and 2.1 kWh/m^2, respectively. In these last months, the appearance of clouds and rain changes affected the solar radiation availability.

The calculated and experimental temperatures of the glass part of the collector as a function of the experimental months are depicted in Figure 4. The maximal experimental temperature of the glass cover takes place in the month of May with 38.7 ºC, however, simulation gives maximal temperatures of 43 ºC. The minimal temperatures are reached in the month of November with a simulated temperature of 32 ºC and an experimental temperature of 25 ºC. This difference could be as a result of the external wind velocities that were not considered in the simulation, and this directly affected the energy transfer to the environment, since there is a convective coefficient due to the wind speed. Despite those differences, the model describes the behavior of the glass cover temperatures well.

Regarding water temperatures inside the equipment, temperature maximum was also achieved in May, both theoretically (40 ºC) and experimentally (44.28 ºC) as it can be seen in Figure 5. The minimal temperatures were reached in November, with a theoretical temperature of 31.15 ºC and experimental

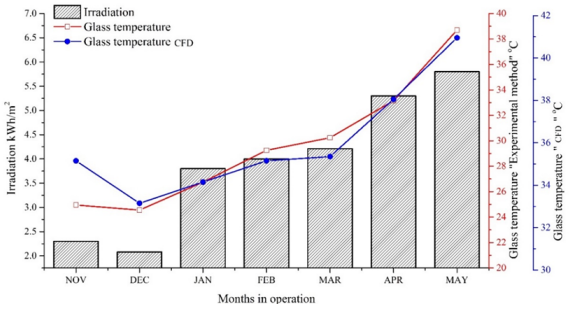

Figure 4. Theoretical and experimental temperatures of the glass as a function of months of operation and incident radiation.

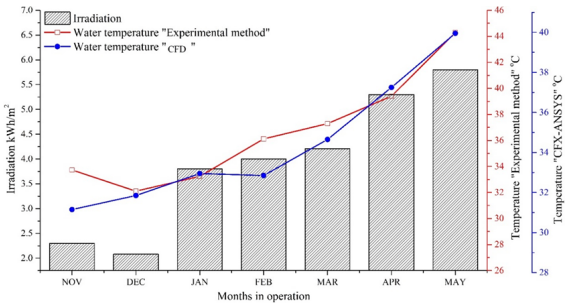

Figure 5. Theoretical and experimental temperatures of the water as a function of months of operation and incident radiation.

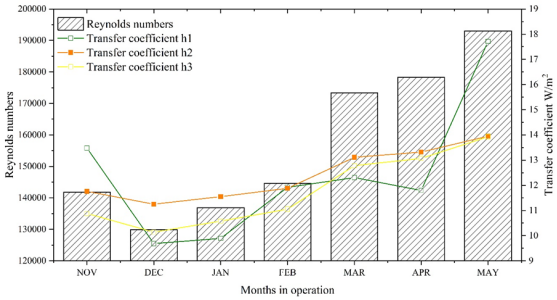

Figure 6. Transfer coefficients with the incident radiation during the period of experimentation as a function of months of operation and Reynolds numbers.

one of 33.73 ºC. In this case, the model also represents well the behavior of the water temperature in the equipment. Water temperature increase as the solar radiation also does. Table 3 shows the results of the cover temperature, the internal temperature and the distilled volume of the experimentation and the CFX simulation.

Figure 6 shows the transfer coefficients obtained during the months of operation. The average results

were obtained for each month of operation, it is observed that the h1 of Eq. 2 behaved accordingly to the water temperature and reached the highest h1 in the month of May with 17.71 W / m^2 and a maximum q1 of 802.43 W / m^2. The lowest h1 was found in December with 9.68 W / m^2 and q1 was at a minimum of 252.49 W / m^2. Constants C = 0.0538 and n = 0.383 as reported by Tiwari and Sanjay (1996) were used to calculate the transfer coefficients. For the case of h2, it was calculated using Eq. 3, which depends on the wind speed; the highest coefficient is presented in May with 13.95 W / m^2 and the lowest transfer coefficient is presented in December with 11.25 W / m^2. As for the transfer coefficient h3 of Eq. 9 it is observed that, as with the previously noted cases, the highest coefficient occurs in the month of May with 13.92 W / m^2 and the lowest coefficient occurs in the month of December with 10.14 W / m^2. The coefficients h2 and h3, behave in a similar way as does the incident radiation which increases according to the increase of Reynolds numbers. However, h1 has a different behavior since it depends on the heat transfer by convection with respect to wind speed and of the incident solar radiation.

In figure 7, the distillate volume and incident radiation during the months of operation are shown. The distillate volume increases as the incident global radiation increases. The highest distillate volume occurs in the month of May with 1000 ml of production and the lowest volume of distillate is presented in December with 822 ml of production. These results coincide with incident solar radiation, which indicates that the quantity of distillate volume behaves in accordance with the incident radiation of the equipment surface.

In Figure 7 is shown a comparison between the average volume generated experimentally with the theoretical volume. The month of May exhibits the maximal experimental amount of distillate with 1000 ml whereas the simulation gives an amount of 942 ml. The lowest volume of distillate is obtained in December with 822 ml, and the model gives an amount of 823 ml. The month of January gives the maximal difference between experimental and theoretical results, with experimental results of 750ml and theoretical results of 6480 ml, a difference of around 13%, this difference appears due to environmental conditions such as ambient temperature, wind speed, relative humidity, since these variables were not taken into account in the CFX simulation. On the other hand, the month of December showed a minor difference with 822 ml of distillate in

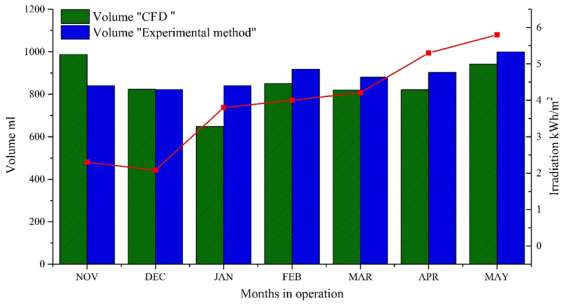

Figure 7. Comparison of the theoretical and experimental distillate volume during the months of operation and incident radiation (right axis).

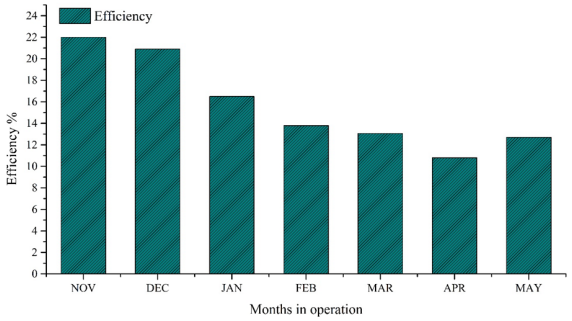

Figure 8. Efficiency of the equipment in the months of operation.

the experimental results and 823 ml of distillate in the simulation results, giving a difference of 0.6%. The month of November presents the biggest difference with 14%, where the experimental method obtained 840 ml and 980 ml in the simulation. Climatic conditions that were not taken into account in the simulation could affect the proximity of the data, such as relative humidity and wind speed, which affect the temperature of the glass cover.

From the information presented in Table 2, a degree of direct linear correlation of approximately 0.80 is obtained with respect to the parameters under study. In table 2, the average of the correlation coefficient per month is presented.

For passive solar distillers the efficiency for solar distillers is 35% (Hermosillo Villalobos, 2013). The efficiency of the solar still prototype used in this work was calculated using Eq.14. In Figure 8 is shown the maximal efficiency is obtained in November with 22% and in December with 20.9%. On the other hand, the minimal efficiency is obtained in April with 10.8%. The average efficiency during the months of operation is 16%. This result is compared to the efficiency obtained by El *et al*. in 2017 who reported

Table 3. Results of the CFX simulation compared to the experimental results.

Month	Glass Temperature Experimental ºC	Glass Temperature CFX ºC	Internal Temperature Experimental ºC	Internal Temperature CFX ºC	Volume Temperature ml	Volume CFX ml
November	29.95	35.15	37.73	31.5	840	987
December	24.55	33.15	32.1	31.85	822	823
January	26.75	34.15	33.24	32.95	750	648
February	29.25	35.15	36.12	32.85	918	851
March	30.24	33.35	37.29	34.65	880	820
April	33.15	38.05	39.4	37.25	903	821
May	38.7	40.95	44.28	39.95	1000	942

Table 4. Analysis results of distilled water.

Parameters		*Seawater*	*Distilled water*	*Drinking water standards NOM-127-SSA1-1994*
pH		6.69	7	6.4 a 8.5
Conductivity (µs/cm)		40000	8.75	≤1000
Turbidity (NTU)		3	1	≤5
Sodium (mg/L)		11433.61	1.86	≤200
Colour		Colorless	Colorless	Colorless
Hardness (mg/L Ca en CaCO3)		3400	1.12	500 mg/L
Microbiological results (CFU/mL)				
Total Coliform	Fecal Coliform	Not detectable	Not detectable	2.0 MPN/100mL

an efficiency of up to 50% in an operating day and those authors obtained an average efficiency of 13 to 14% (El *et al*., 2017).

However, the computational modeling gives the guidelines to increase the efficiency, since modifications and improvements to the design can be proposed. For example, the increase of the condensate velocity from the cooling of the glass could be modified since it has been observed that a greater difference between the temperature of the water and the temperature of the glass cover increases the amount of distilled volume. Starting from this idea can increase the internal temperature from the preheating of water with different systems, such as the use of evacuated tubes or from the residual heat of another process. Construction materials and dimensions are an important point for the redesign of passive solar distillers, hence it is important to find or synthesize highly efficient materials with high thermal conductivity that are highly resistant to corrosion by the dissolved salts present in the water.

Its thermal efficiency was determined from the measurement of the incident radiation at the site, the area of the collector and the amount of distilled water produced in a day. Equation 22 shows the relationship of these variables. The efficiency determination was carried out on a monthly average where the behavior of the temperature and the amount of fresh water that the team produced throughout the experimentation was observed. It was possible to observe which variables and factors decrease the efficiency of the equipment and at which stage of the year these devices have the greatest use of heat.

$$\eta = \frac{m_w * \Delta H_{vap}}{H_s A * 3600} \tag{22}$$

Where η is the thermal efficiency of the solar distiller, m_w is the distillate mass, ΔH_{vap} is the latent vaporization coefficient, H_s is the incident radiation.

It is observed that for the increase of the temperature of the cover and of the internal water, increasing as the incident radiation increases, the heat transfer coefficients behave in a similar manner, except for the one that depends on the internal temperature of glass. The amount of distillate is directly related to

the above variables, indicating that for higher distillate production a high heat transfer required in the different components of the distillation equipment.

Moreover, during the experiments, in order to determine the drinkability of distilled water obtained from a solar distiller, the water samples taken from distilled water under hygienic conditions were analyzed in laboratory, and the results are presented in Table 4. In Table 4, it is seen that the water meets the NOM-127-SSA1-1994 standard.

Conclusions

The cover and water internal temperatures increase as the incident radiation increases. Heat transfer coefficients behave similarly, but depending also on glass internal temperature. The amount of distillate is directly related to the above variables, indicating that for larger distillate production, a high heat transfer is required among the different components of the distillation equipment.

The CFX simulation shows the behavior of the distillation equipment in obtaining water and the temperature of the glass and water. Differences were observed between the experimental method and the simulation in CFX; in the case of water temperature the difference was 5.8% and in the case of the distiller volume it was 8.2%.

The efficiency of the equipment is within the parameters reported by other authors. However, it was observed that the climatic conditions can affect the behavior of the solar distiller. The key factor for high efficiency is the radiation, but wind speed and ambient temperature can affect the system yield. The results in CFD have a slight difference with respect to the experimental results, and this provides the opportunity for improvements to increase the efficiency of the equipment, either with the addition of new components to carry out forced convection or for the addition of heat in the system or the improvement of construction materials. Likewise, the distilled water can be produced in regions with lack of potable water.

Acknowledgements

This work was supported by the CONACYT (No.550281), El Programa de Fortalecimiento de la Calidad Educativa (PFCE) (2015-2016).

Nomenclature

Cp_c	Specific heat of the steel container J/Kg K
Cp_g	Specific heat of the glass cover J/KgK
Cp_w	Specific heat of the water J/KgK
Gr	Grashof number Dimensionless
g	Gravity m/s^2
H_s	Incident radiation in the cover kWh/m^2
h_1	Convective coefficient water-glass W/m^2
h_2	Heat transfer coefficient glass-environment W/m^2
h_3	Heat transfer coefficient container-water W/m^2
h_4	Heat transfer coefficient container-environment W/m^2
k_{air}	Thermal conductivity of air W/mK
k_w	Thermal conductivity of water W/mK
l	Length of the glass m
lw	Length of the container m
m_c	Mass of the container kg
m_g	Mass of the glass kg
m_w	Mass of the water kg
Nu	Nulsset number Dimensionless
p_g	Saturated vapor pressure at temperature of glass atm
p_w	Saturated vapor pressure at temperature of water atm
Pr	Prandtl number Dimensionless
$q1$	Convective heat transfer rate from water to the glass surface W/m^2
Tc	Container temperature K
Te	Environment temperature K
Tg	Glass temperature K
Tw	Water temperature K
α_1	Absorption coefficient of the glass kWh/m^{2}K
α_2	Absorption coefficient of the water kWh/m^{2}K
α_3	Absorption coefficient of the steel kWh/m^{2}K
β	Volumetric expansion coefficient K^{-1}
ρ	Water density Kg/m^3
μ	Kinematic viscosity water m^2/s
η	Efficiency %
ΔH_{vap}	Latent heat of vaporization kJ/kg

References

Abdel-Rehim, Z. S., & Lasheen, A. (2005). Improving the performance of solar desalination systems. *Renewable Energy 30*, 1955-1971. doi: http://dx.doi.org/10.1016/j.renene.2005.01.008

Al-Nimr, M. d. A., & Dahdolan, M. d.-E. (2015). Modeling of a novel concentrated solar still enhanced with a porous evaporator and an internal condenser. *Solar Energy 114*, 8-16. doi: https://doi.org/10.1016/j.solener.2015.01.021

Al-Sulttani, A. O., Ahsan, A., Rahman, A., Nik Daud, N. N., & Idrus, S. (2017). Heat transfer coefficients and yield analysis of a double-slope solar still hybrid with rubber scrapers: An experimental and theoretical study. *Desalination 407*, 61-74. doi: https://doi.org/10.1016/j.desal.2016.12.017

Banat, F., Jumah, R., & Garaibeh, M. (2002). Exploitation of solar energy collected by solar stills for desalination by membrane distillation. *Renewable Energy 25*, 293-305. doi: http://dx.doi.org/10.1016/S0960-1481(01)00058-1

Çengel, Y. A., & Ghajar, A. J. (2011). *Heat and Mass Transfer: Fundamentals & Applications*. McGraw-Hill.

Çengel, Y. A., & Ghajar, A. J. (2011). *Transferencia de calor y masa*.McGraw-Hill.

CONAGUA. (2012). http://www.conagua.gob.mx/atlas/.

Duffie, J. A., Beckman, W. A., & Worek, W. (2013). *Solar Engineering of Thermal Processes* (Vol. 3): Wiley Online Library.

Dunkle, R. (1961). Solar water distillation. The roof type still and a multiple effect diffusion still. *International Developments in Heat Transfer*. ASME, Proceeding of International Heat Transfer, Part V, University of Colorado.

Dunkle, R. V., CSIRO, Scientific, C., & Organization, I. R. (1961). *Solar Water Distillation: The Roof Type Still and a Multiple Effect Diffusion Still*. C.S.I.R.O.

El, E., Çakmak, G., & Yildiz, C. (2017). Efficiency analysis of tank-type water distillation system integrated with hot water collector. *Thermal Science and Engineering Progress 3*, 24-30. doi: https://doi.org/10.1016/j.tsep.2017.05.012

Elashmawy, M. (2017). An experimental investigation of a parabolic concentrator solar tracking system integrated with a tubular solar still. *Desalination 411*, 1-8. doi: https://doi.org/10.1016/j.desal.2017.02.003

Fernández, J., & Chargoy, N. (1990). Multi-stage, indirectly heated solar still. *Solar Energy 44*, 215-223. doi: http://dx.doi.org/10.1016/0038-092X(90)90150-B

Gomez-Daza, J. C., & Ochoa-Martinez, C. I. (2011). Computational fluid dynamics in drying and cooling operations applied to the food industry. *Ingeniería y Competividad 13*, 103-114.

González, F. (2014). Análisis de las variables medidas en una estación anemo-solarimétrica, para la evaluación del recurso solar y eólico en la ciudad de Tepic, Nayarit. Autonomous University of Nayarit, Nayarit, México.

Guide, A. C.-S. M. J. A. I. (2012). Release 14.5.

Hermosillo Villalobos, J. J. (2013). Estudio de la transferencia de calor en un sistema desalinizador mediante humidificación y deshumidificación de aire. (Phd), UNAM,

INIFAP. (2014). Instituto Nacional de Investigaciones Forestales, Agricolas y Pecuarias. Retrieved from http://clima.inifap.gob.mx

Kaushal, A. K., Mittal, M. K., & Gangacharyulu, D. (2017). An experimental study of floating wick basin type vertical multiple effect diffusion solar still with waste heat recovery. *Desalination 414*, 35-45. doi: https://doi.org/10.1016/j.desal.2017.03.033

Khare, V. R., Singh, A. P., Kumar, H., & Khatri, R. (2017). Modelling and performance enhancement of single slope solar still using CFD. *Energy Procedia 109*, 447-455. doi: https://doi.org/10.1016/j.egypro.2017.03.064

Kumar, S., & Tiwari, G. N. (1996). Estimation of convective mass transfer in solar distillation systems. *Solar Energy 57*, 459-464. doi: https://doi.org/10.1016/S0038-092X(96)00122-3

PNUMA. (2012). Medio ambiente para el futuro que queremos. Retrieved from http://www.unep.org/geo/pdfs/geo5/GEO5_report_full_es.pdf

Rahbar, N., Asadi, A., & Fotouhi-Bafghi, E. (2018). Performance evaluation of two solar stills of different geometries: Tubular versus triangular: Experimental study, numerical simulation, and second law analysis. *Desalination 443*, 44-55. doi: https://doi.org/10.1016/j.desal.2018.05.015

Rahbar, N., Esfahani, J. A., & Fotouhi-Bafghi, E. (2015). Estimation of convective heat transfer coefficient and water-productivity in a tubular solar still-CFD simulation and theoretical analysis. *Solar Energy 113*, 313-323. doi: http://dx.doi.org/10.1016/j.solener.2014.12.032

Ranjan, K. R., & Kaushik, S. C. (2013). Energy, exergy and thermo-economic analysis of solar distillation systems: A review. *Renewable and Sustainable Energy Reviews 27*, 709-723. doi: http://dx.doi.org/10.1016/j.rser.2013.07.025

Rashidi, S., Rahbar, N., Valipour, M. S., & Esfahani, J. A. (2018). Enhancement of solar still by reticular porous media: Experimental investigation with exergy and economic analysis. *Applied Thermal Engineering 130*, 1341-1348. doi: https://doi.org/10.1016/j.applthermaleng.2017.11.089

Reyes-Vidal, M. Y., Diez, Á. A., Martínez-Silva, A., & Asaff, A. (2012). Investigación, desarrollo tecnológico e innovación para el cuidado y reuso del agua. (Spanish). *Research, Technology Development and Innovation for Water Saving and Recycling 2*, 199-216.

Sampathkumar, K., Arjunan, T. V., Pitchandi, P., & Senthilkumar, P. (2010). Active solar distillation-A detailed review. *Renewable and Sustainable Energy Reviews 14*, 1503-1526. doi: https://doi.org/10.1016/j.rser.2010.01.023

Samuel Hansen, R., & Kalidasa Murugavel, K. (2017). Enhancement of integrated solar still using different new absorber configurations: An experimental approach. *Desalination 422*, 59-67. doi: https://doi.org/10.1016/j.desal.2017.08.015

Sharpley, B., Boelter, L. J. I., & Chemistry, E. (1938). Evaporation of water into quiet air from a one-foot diameter surface. *Industrial and Engineering Chemistry 30*, 1125-1131.

Singh, A. K., Singh, D. B., Mallick, A., Harender, Sharma, S. K., Kumar, N., & Dwivedi, V. K. (2019). Performance analysis of specially designed single basin passive solar distillers incorporated with novel solar desalting stills: A review. *Solar Energy 185*, 146-164. doi: https://doi.org/10.1016/j.solener.2019.04.040

Singh, A. K., Singh, D. B., Mallick, A., & Kumar, N. (2018). Energy matrices and efficiency analyses of solar distiller units: A review. *Solar Energy 173*, 53-75. doi: https://doi.org/10.1016/j.solener.2018.07.020

Susana Fonseca, Eider Miranda, & Torres, A. (2012). Mathematical model and analitycal solution of operation of a solar pan. *Tecnología Química 32*, 154-161.

Tripathi, R., & Tiwari, G. N. (2006). Thermal modeling of passive and active solar stills for different depths of water by using the concept of solar fraction. *Solar Energy 80*, 956-967. doi: https://doi.org/10.1016/j.solener.2005.08.002

Tsilingiris, P. T. (2013). The application and experimental validation of a heat and mass transfer analogy model for the prediction of mass transfer in solar distillation systems. *Applied Thermal Engineering 50*, 422-428. doi: https://doi.org/10.1016/j.applthermaleng.2012.07.007

Tutorials, A. R. (2015). Wall Condensation Model. Retrieved from https://www.sharcnet.ca/Software/Ansys/16.2.3/en-us/help/cfx_thry/wall_con_mass_trans.html#eq_wall_con_2114

Watmuff, J., Charters, & Proctor. (1977). Solar and wind induced external coefficients

for solar collectors. *Revue Internationale D'Heliotechnique 2*, 56.